

Magnetic power spectra from Faraday rotation maps

REALMAF and its use on Hydra A

Petr Kuchar and Torsten Enßlin

Max Planck Institute for Astrophysics

Preprint online version: November 1, 2018

ABSTRACT

We develop a novel maximum a posterior method to measure magnetic power spectra from Faraday rotation data and implement it in the REALMAF code. Using a sophisticated model for the magnetic autocorrelation in real space permits us to alleviate previously required simplifying assumptions in the processing. We also introduce a way to treat the divergence relation of the magnetic field with a multiplicative factor in Fourier space, which allows us to model the magnetic autocorrelation as a spherically symmetric function. Applied to the dataset of Hydra A north, we find a power law power spectrum between spatial scales of 0.3 kpc to 8 kpc, with no visible turnover at large scales within this range and a spectral index consistent with a Kolmogorov-like power law regime. The magnetic field strength profile seems to follow the electron density profile with an index $\alpha = 1$. A variation of α from 0.5 to 1.5 would lead to a spectral index between 1.55 and 2.05. The extrapolated magnetic field strength in the cluster center highly depends on the assumed projection angle of the jet. For an angle of 45° we get $36 \mu\text{G}$ in the center and directly probed $16 \mu\text{G}$ at 50 kpc radius.

Key words. galaxy clusters – magnetic fields – Faraday rotation

1. Introduction

Intergalactic magnetic fields are of great scientific interest. They are part of the intergalactic metabolism, they affect the propagation of heat and cosmic rays, and they are tracers of the dynamical state of the intergalactic medium. One way to retrieve their properties is to measure the Faraday rotation effect they cause on traversing polarized light. This has led to a great deal of insight into the presence, strength and morphology of magnetic fields in galaxy clusters.¹

The polarization of light traveling through a magnetized plasma is affected by the wavelength-dependent Faraday rotation effect producing a change in polarization angle $\Delta\phi$:

$$\Delta\phi(\mathbf{x}_\perp) = \lambda^2 a_o \int_{z_1}^{\infty} n_e(\mathbf{x}_\perp, z) \cdot B_z(\mathbf{x}_\perp, z) dz \equiv \lambda^2 \text{RM}(\mathbf{x}_\perp), \quad (1)$$

with a proportionality constant $a_o = e^3 / (2\pi m_e^2 c^4)$. This was accurately measured in the Hydra A galaxy cluster by Taylor & Perley (1993). The cluster space is filled with plasma with the electron density $n_e(\mathbf{x}_\perp, z)$ centered around a cD galaxy hosting a supermassive black hole. Hydra A is a radio galaxy with out-streaming jets, which inflate bubbles filled with relativistic, radio emitting plasma. This is visible as cavities in the X-ray emission of the surrounding hot cluster atmosphere. The radio emission of the bubbles is polarized. On the way to the

¹ Some of the many studies in this directions are Dennison (1979), Lawler & Dennison (1982), Dreher et al. (1987), Laing (1988), Hennessy et al. (1989), Taylor et al. (1990), Goldshmidt & Rephaeli (1993), Kim et al. (1991), Ge & Owen (1994), Feretti et al. (1995), Johnson et al. (1995), Johnson et al. (1995), Feretti et al. (1999a,b), Clarke et al. (2001), Taylor et al. (2001), Carilli & Taylor (2002), Taylor et al. (2002), Eilek & Owen (2002), Enßlin et al. (2003) and Murgia et al. (2004), Laing et al. (2006), Xu et al. (2006), Taylor et al. (2007), Cho & Ryu (2009), Feain et al. (2009), Battaglia et al. (2009), where we omitted the works directly addressed in the following.

observer the light travels through the magnetized intra-cluster medium with the magnetic field $B(\mathbf{x}_\perp, z)$, where the Faraday rotation effect changes its polarization. Measuring the polarized intensity P and finding a linear relation between P and λ^2 verifies that Faraday rotation occurs in the foreground medium and not in the source of the polarized light, where the electron density n_e is negligible small. Therefore the values $\Delta\phi/\lambda^2$ of a 2-dimensional rotation measure map $\text{RM}(\mathbf{x}_\perp)$ carry valuable information about the intra cluster magnetic fields, as imprinted according Eq. 1.

Due to the information lost in the projection, Eq. 1 is not directly invertible to calculate the line of sight magnetic field B_z in terms of RM and the known electron density profile. But assuming statistical isotropy of the magnetic fields and using a statistical approach we are able to retrieve the amplitude spectrum of the magnetic field in Fourier space, the magnetic power spectrum $\omega(k) = \langle \mathbf{B}(\mathbf{k}) \cdot \overline{\mathbf{B}}(\mathbf{k}) \rangle$, as well the typical field strength B in position space and its autocorrelation length λ_B .

We model the magnetic powerspectrum as a combination of spectral basis functions

$$\omega(k) = \sum_i s_i w_i(k) \quad (2)$$

where the spectral amplitudes form our signal $s = (s_i)$. A probability function for s given the data d , the posterior $P(s|d)$, is set up in terms of $\omega(k)$. Maximizing the posterior retrieves $\omega(k)$, which consists of relatively independent frequency bands. A similar approach has been already applied by Vogt & Enßlin (2005). Expressing the spectral basis functions as analogous basis functions for the magnetic autocorrelation allows us to calculate the RM correlation matrix completely in position space, which makes two rough simplifications in the processing used by Vogt & Enßlin (2005) unnecessary (see Section 4 for further discussion). Moreover we include noise effects into the analysis and model the Faraday screen more accurately using recently

improved measurements of the geometry of the cavities in the Hydra A cluster by Wise et al. (2007).

The Hydra A cluster has been investigated by Laing et al. (2008) as well. They compared simulated rotation measure structure functions with the observed ones. A comparison with their results will be discussed in Section 4.

Another approach for retrieving magnetic power spectra is that proposed by Murgia et al. (2004). Assuming a power law power spectrum, they simulated Faraday rotation maps by using the FARADAY code and compared the observed and synthetic profiles of the dispersion of the RM as fit criterion. In order to find a good fit (Murgia et al. 2004) assume a power law to restrict the number of degrees of freedom. This method was also applied e.g. by Govoni et al. (2006) and Guidetti et al. (2008).

In this work, we present the code REALMAF², which should alleviate several of the restrictions and assumptions of former approaches. Although REALMAF also requires the spectral range to be set up by hand, the posterior statistics calculated by it guides the choice. The power spectrum within the chosen range is relatively free to adopt any slope required by the data and permitted by the number of assumed spectral bands. The automatically obtained statistical deviations of the spectral amplitudes s_i are negligible in the center of the spectral range of the power spectrum for the case of Hydra A considered here. Thus, no smoothness enforcing coupling between the spectral bands is necessary in REALMAF.

Our method relies on the following information and assumptions:

- The rotation measure map and its error map,
- knowledge of the geometry of the Faraday active volume, which depends also on the projection angle θ of the jet and the cavity size,
- knowledge of the electron density profile n_e ,
- assuming that the magnetic field strength B follows the electron density profile like $B \propto n_e^\alpha$ (e.g. Dolag et al. 2001),
- assuming statistical isotropy of B ,
- assuming solenoidal fields
- assuming that there is no polarized radio emission inside of the Faraday active volume in front of the radio bubble,
- assuming a Gaussian probability distribution of the rotation measure map.

Although it is not possible to retrieve the exact magnetic field in position space, the accessible power spectrum is a valuable information and contains information on the typical field strength, correlation length and the distribution of magnetic energy onto different length-scales. All these quantities can be predicted in magneto-genesis theories. The latter, the spectral energy distribution is a sort of fingerprint of such theories. E.g. magneto-genesis-scenarios in which the energy is injected on large scales by gas stirring typically exhibit Kolmogorov-like power law spectra (Subramanian et al. 2006; Enßlin & Vogt 2006). Scenarios, where the magnetic fields are build up from small to large scales may exhibit different spectral slopes (Schekochihin & Cowley 2006). Magnetic field measurement by Faraday rotation have therefore the potential to discriminate such theories. We use $H_0 = 70 \text{ km s}^{-1} \text{ Mpc}^{-1}$, $\Omega_m = 0.3$, $\Omega_\Lambda = 0.7$ and a redshift of 0.0538 for Hydra A (de Vaucouleurs et al. 1991). To follow the tradition in cosmic magnetism studies we use cgs-units in this paper with the energy unit $1 \text{ erg} = 10^{-7} \text{ Joule}$ and magnetic field strength unit $1 \text{ G} = 10^{-4} \text{ T}$.

2. Method

2.1. Statistical basics

Our aim is to retrieve from the rotation measure (data d) the magnetic power spectrum represented by the spectral amplitudes (signal s). Bayes theorem expresses the posterior $P(s|d)$ (the conditional probability of the signal given the data) in terms of the likelihood $P(d|s)$ in the following way:

$$P(s|d) = \frac{P(d|s) \cdot P(s)}{P(d)} \quad (3)$$

Since $P(d)$ is a constant, the most probable s given d can be retrieved by maximizing the joint probability consisting of the likelihood $P(d|s)$ multiplied with the Prior $P(s)$. Here we adopt Jeffrey's prior, $P(s) \propto s^{-1}$, which is a uniform distribution on logarithmic scale. Assuming a Gaussian distribution of the magnetic field, which results in a Gaussian probability distribution of RM values³ centered on zero for all entries of the rotation measure map, makes the likelihood a Gaussian. Thus it can be expressed in terms of the correlation matrix $C = \langle d_i d_j \rangle$, with data d being a vector of length n :

$$P(d|s) = \frac{1}{(2\pi)^{\frac{n}{2}} |C|^{\frac{1}{2}}} e^{-\frac{1}{2} d^T C^{-1} d}. \quad (4)$$

An expression for $C \equiv C(s) = \langle d_i d_j \rangle$ needs to be derived in the following.

In the view of the linearity of Eq. 1, the data can be expressed in terms of the magnetic field B (vector over physical space), a response matrix R (projecting from physical to data space) and noise n (in data space) as: $d = RB + n$. From this we find

$$C(s) = \langle (RB + n)(RB + n)^T \rangle = R \langle BB^T \rangle R^T + \langle nn^T \rangle \equiv \tilde{C}(s) + N$$

Thus to any derived Faraday rotation correlation matrix $\tilde{C}(s)$ a good estimate for the noise matrix N needs to be added.

2.2. Maximizing the posterior

The power spectrum inference within the maximum a posterior approach can only be conducted numerically. Here, we maximize the logarithm of the posterior, since there are convenient analytical expressions for the gradient and Hessian. Multiplication of the likelihood with the prior to get the posterior is an addition in logarithmic space, which also simplifies matters. Indices i, j refer to the degrees of freedom of the parameterization of s . We find

$$\frac{\partial \ln[P(s|d)]}{\partial s_i} = \frac{1}{2} \text{Tr}[(dd^T - C)(C^{-1} \frac{\partial C}{\partial s_i} C^{-1})] - \frac{1}{s_i}, \quad (5)$$

and if s contributes only linearly to \tilde{C} :

$$\begin{aligned} \frac{\partial^2 \ln[P(s|d)]}{\partial s_j \partial s_i} = & -\frac{1}{2} \text{Tr}[C^{-1} \frac{\partial C}{\partial a_j} C^{-1} \frac{\partial C}{\partial s_i}] \\ & - \text{Tr}[(dd^T - C)(C^{-1} \frac{\partial C}{\partial s_i} C^{-1} \frac{\partial C}{\partial s_j} C^{-1})] + \frac{\delta_{ij}}{s_i^2}. \end{aligned} \quad (6)$$

The most probable power spectrum is then found iteratively. We use a second order Newton method to solve for it, with

$$s_{\text{new}} = s - \left(\frac{\partial^2 \ln[P(s|d)]}{\partial s_j \partial s_i} \right)^{-1} \frac{\partial \ln[P(s|d)]}{\partial s_i}$$

³ This is valid to lowest order in our knowledge, and also motivated by the central limit theorem of statistics.

² REAL MAGnetic Fields

2.3. The correlation matrix

An expression for the correlation matrix $\tilde{C} = \langle \text{RM}(\mathbf{x}_\perp) \cdot \text{RM}'(\mathbf{x}'_\perp) \rangle$ of the rotation measure map needs to be derived in the following form.

$$\tilde{C}(\mathbf{x}_\perp, \mathbf{x}'_\perp) = \langle a_o^2 \int_{z_1}^{\infty} n_e(\mathbf{x}) B_z(\mathbf{x}) dz \int_{z_2}^{\infty} n_e(\mathbf{x}') B_z(\mathbf{x}') dz' \rangle$$

The electron density distribution $n_e(\mathbf{x})$ needs to be obtained from independent data, e.g. from X-ray observations. The magnetic field energy is assumed to follow $n_e(\mathbf{x})$ with:

$$\langle B^2(\mathbf{x}) \rangle = B_o^2 (n_e(\mathbf{x})/n_o)^{2\alpha} \quad (7)$$

(Dolag et al. 2002). The following approach is based on statistical homogeneity of the magnetic field. Therefore we rescale $\langle B^2(\mathbf{x}) \rangle$ with a rescale function h , $h(\mathbf{x}) = \langle B^2(\mathbf{x}) \rangle^{0.5} / B_o = (n_e(\mathbf{x})/n_o)^\alpha$. This ensures $\langle \tilde{B}^2(x) \rangle = \langle B^2(\mathbf{x}) \rangle / h^2(\mathbf{x}) = B_o^2$ to be independent of position. If we also assume statistical isotropy we get the scaling of the required z-component of B: $\langle B_z^2(\mathbf{x}) \rangle / B_o^2 = \langle B^2(\mathbf{x}) \rangle / B_o^2$. Thus,

$$\begin{aligned} \tilde{C} &= a_o^2 \int_{z_1}^{\infty} n_e(\mathbf{x}_\perp, z) h(\mathbf{x}_\perp, z) \\ &\cdot \int_{z_2}^{\infty} n_e(\mathbf{x}'_\perp, z') h(\mathbf{x}'_\perp, z') \langle \tilde{B}_z(\mathbf{x}_\perp, z) \tilde{B}_z(\mathbf{x}'_\perp, z') \rangle dz dz' \quad (8) \\ &= a_o^2 n_o^2 \int_{z_1}^{\infty} f(\mathbf{x}_\perp, z) \int_{z_2-z}^{\infty} f(\mathbf{x}'_\perp, r_z + z) M_{zz}(\mathbf{r}) dr_z dz \end{aligned}$$

with $\mathbf{r} = (\mathbf{x}_\perp - \mathbf{x}'_\perp, r_z)$, where we introduced the window function f which is nonzero inside the Faraday screen:

$$f(\mathbf{x}) = \frac{n_e(\mathbf{x})}{n_o} h(\mathbf{x}) = \left(\frac{n_e(\mathbf{x})}{n_o} \right)^{\alpha+1} \quad (9)$$

$M_{zz}(\mathbf{r}) = \langle \tilde{B}_z(\mathbf{x}) \tilde{B}_z(\mathbf{x} + \mathbf{r}) \rangle$ is the zz -part of the magnetic autocorrelation tensor.

2.4. Modeling the magnetic autocorrelation

$M_{zz}(\mathbf{r})$ can be split up into a longitudinal part $M_L(r)$ and a corresponding perpendicular part $M_N(r)$, which depend only on the absolute value of \mathbf{r} , see Subramanian (1999) or Enßlin & Vogt (2003).

$$M_{zz}(\mathbf{r}) = M_L(r) \frac{r_z^2}{r^2} + M_N(r) \frac{r_\perp^2}{r^2} \quad (10)$$

The rescaled magnetic autocorrelation function $\omega(r) = \langle \tilde{B}(\mathbf{x}) \cdot \tilde{B}(\mathbf{x} + \mathbf{r}) \rangle$ is given by:

$$\omega(r) = \sum_k M_{kk} = 2M_N(r) + M_L(r) \quad (11)$$

The information of the data can be combined into a one-dimensional correlation function and therefore does not allow to determine simultaneously two independent functions. Thus a relation between M_N and M_L is necessary. There are two suitable possibilities how to connect them.

a) Full isotropy assumption, which additionally assumes isotropy at any location in Fourier space. This yields:

$$M_N(r) = M_L(r) \quad (12)$$

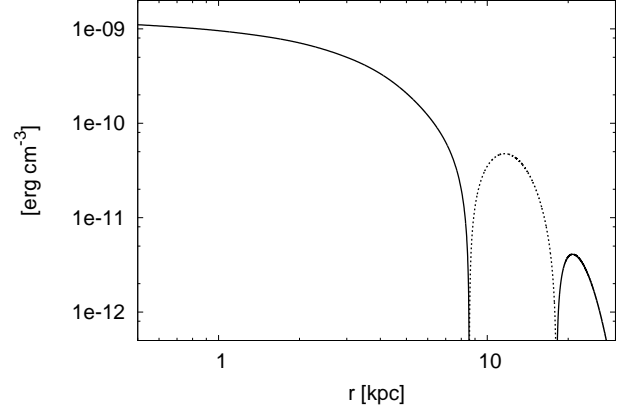


Fig. 1: Magnetic autocorrelation $\omega(r)$ in position space. The negative part of $\omega(r)$. (7 spectral bins, $\theta = 45^\circ$ and $\alpha = 1$)

b) Considering the solenoidal character of the magnetic field by $\nabla \cdot \tilde{B} = 0$, which yields:

$$M_N(r) = \frac{1}{2r} \frac{d}{dr} (r^2 M_L(r)) \quad (13)$$

The $\nabla \cdot \tilde{B} = 0$ condition is more physical, but also more complicated to handle. Both assumptions have been implemented in REALMAF. However, the most computational efficient way is to use the full isotropy assumption and apply the divergence relation in Fourier space, which results in a simple multiplication factor, see Section 2.5.

Connecting of M_L and M_N allows to parameterize $M_{zz}(r)$ using:

$$M_{zz}(\mathbf{r}) = \sum_i s_i M_{zz}^{(i)}(\mathbf{r}), \quad (14)$$

where $M_{zz}^{(i)}(\mathbf{r})$ is further split into $M_L^{(i)}(r)$ and $M_N^{(i)}(r)$ described by Eq. 10. Because of linearity of the Fourier transformation, the linear coefficients s_i in real space also appear as linear coefficients in the analogous representation in Fourier space. So although we are calculating the correlation matrix completely in real space, the power spectrum can directly be obtained:

$$\omega(k) = \sum_i s_i (2M_N^{(i)}(k) + M_L^{(i)}(k)) = \sum_i s_i w_i(k)$$

The basis functions together with the retrieved spectral amplitudes s_i can be translated into $\omega(r)$ as seen in Fig. 1 and the corresponding $\omega(k)$. The used model functions for $M_N^{(i)}$ and $M_L^{(i)}$ have been chosen to transform into relatively well separated and well located frequency bands $w_i(k)$ in Fourier space as seen in Fig. 2. Appendix A shows the used model functions and describes how they have been derived.

2.5. The divergence relation in Fourier space

The zz -part of the magnetic autocorrelation tensor can be expressed in Fourier space analogously to Eq. 10:

$$M_{zz}(\mathbf{k}) = \widehat{M}_L(k) \frac{k_z^2}{k^2} + \widehat{M}_N(k) \frac{k_\perp^2}{k^2}, \quad (15)$$

Applying $\nabla \cdot \tilde{B} = 0$ gives then:

$$\widehat{M}_L(k) = 0 \implies \widehat{\omega}(k) = 2\widehat{M}_N(k), \quad (16)$$

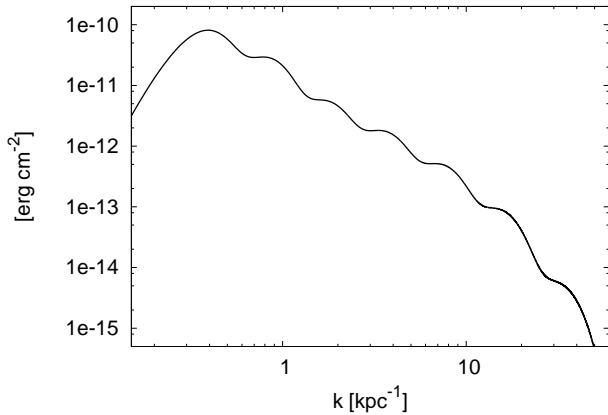


Fig. 2: Magnetic power spectrum $\omega(k)$ in Fourier space transformed into one dimension. The wiggles are due to the seven basis functions of our parameterization. (7 spectral bins, $\theta = 45^\circ$ and $\alpha = 1$)

see Enßlin & Vogt (2003). The $\widehat{M}_L(k)$ from Eq. 15 is in general not the Fourier transformation of $M_L(r)$ used in Eq. 10. To create a connection to the real-space parameterization $M_{zz}(\mathbf{r})$, we multiply $\widehat{\omega}(k)$ by $3/2$ which is analogous to an addition of $\widehat{M}_L(k)$ with $\widehat{M}_L(k) = \widehat{M}_N(k)$. This makes $M_{zz}(\mathbf{k})$ a spherically symmetric function, which forces that its Fourier back-transform $M_{zz}(\mathbf{r})$ must be spherically symmetric as well. Then,

$$M_L(r) = M_N(r) \iff \widehat{M}_L(k) = \widehat{M}_N(k), \quad (17)$$

which is the full isotropy assumption defined in Eq. 12. Therefore when assuming full isotropy, the divergence condition can be imposed on $\omega(k)$ to a good approximation via multiplying it with the factor $2/3$. This has been verified also by numerical experiments.⁴

Using the full isotropy assumption reduces the processing time by up to a factor 4 and allows a simpler spherically symmetric model for M_{zz} . In practice the power spectrum is multiplied with a factor $2/3$ and the resulting magnetic field strength by $\sqrt{2/3}$.

At last we should mention, that the $\nabla \cdot \widetilde{B} = 0$ condition, which is used by Vogt & Enßlin (2005) as well, is not exact because of:

$$\nabla \cdot \widetilde{B} = h \nabla \cdot B + B \cdot \nabla h = B \cdot \nabla h,$$

with the rescale function h defined in section 2.3. In case that B varies on scales much smaller than the ones on which h varies, this assumption is equivalent to the condition $\nabla \cdot B = 0$. Another indication that the resulting errors are negligible small is that a totally different assumption on the statistical distribution of the magnetic fields, like full isotropy, which violates $\nabla \cdot \widetilde{B} = 0$ by definition, produces only a shift by a factor of 1.5 as shown above.

3. Application to the Hydra A data

3.1. The data

We apply REALMAF to the North lobe of the Hydra A galaxy. The original polarization measure map from Taylor & Perley (1993) and Vogt et al. (2005) is translated using the algorithm PACERMAN (Dolag et al. 2005) by doing a linear fit between λ^2

⁴ Actually this relation was discovered in numerical experiment first.

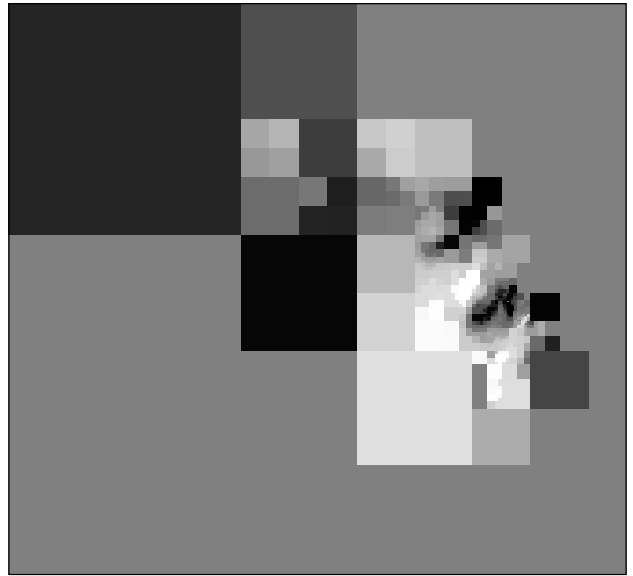


Fig. 3: Merged data map of Hydra A for 1000 data points. The RM values range between -1700 rad/m^2 (dark) and 2800 rad/m^2 (light). The map has a size of about 40 kpc.

and the polarization $\Delta\phi$ producing a rotation measure map and the corresponding error map, see Eq. 1. The resolution of this map is too high to take every single pixel into account in our analysis. Bottleneck is the double integral in the calculation of the model covariance matrix and followed by matrix multiplications in Section 2.2. To reduce the amount of required computational resources, we merge areas in the map to bigger pixels by combining: the rotation measure values, the errors and the pixel position in an inverse noise weighted fashion like Vogt & Enßlin (2005). These merged data points then form the data vector d used in section 2.1. Figure 3 visualizes the merged map.

We also require a noise covariance matrix. Assuming the noise at different pixels to be uncorrelated, the noise matrix is diagonal. The diagonal elements can be approximated by the square of the RM-deviation of each pixel given by the error map produced by PACERMAN.

The used rotation measure map has a mean value of about $600 \frac{\text{rad}}{\text{m}^2}$. The galactic rotation measure at the position of Hydra A is about 1 percent of this and therefore negligible, see Johnston-Hollitt et al. (2004). Therefore we assume that the mean value is due to cosmic variance caused by processing a too small sample of the cluster. This mean value gets correctly interpreted by our method and just lifts the lowest wave-vector part of the magnetic power spectra, compared to the case in which we subtract the mean value from the data d .

3.2. Window function

The window function f defined in Eq. 9 requires the electron density distribution $n_e(x)$. Hydra A is a cooling core cluster. Therefore we assume a spherically symmetric double beta profile defined as:

$$n_e(x) = [n_{e1}^2(1 + (\frac{r}{r_{c1}})^2)^{-3\beta} + n_{e2}^2(1 + (\frac{r}{r_{c2}})^2)^{-3\beta}]^{1/2} \quad (18)$$

with $n_{e1} = 0.056 \text{ cm}^{-3}$, $n_{e2} = 0.0063 \text{ cm}^{-3}$, $r_{c1} = 33.3 \text{ kpc}$, $r_{c2} = 169 \text{ kpc}$ and $\beta = 0.766$, as fitted by Vogt & Enßlin (2005) using data from Mohr et al. (1999). Various works propose that

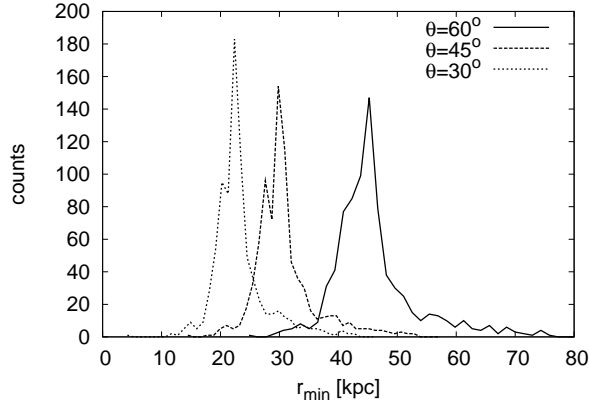


Fig. 4: Histogram of the minimal distance r_{min} from cluster center for 800 data points depending on the assumed projection angle θ . Magnetic fields at $r < r_{min}$ are invisible to the method.

the observed radio lobes of active galactic nuclei, like Hydra A, form cavities in the cluster atmosphere, e.g. see Boehringer et al. (1993), Enßlin (1999), McNamara et al. (2000), Fabian et al. (2000), David et al. (2001). In these cavities the polarized radio light is produced, but $n_e(x)$ is practically 0, so no Faraday rotation occurs there. The fact $n_e(x) = 0$ for any $x \in$ cavity can be taken into account by adjusting the integration boundaries in Eq. 8. In order to calculate the important lower integration boundary, where the Faraday active area starts, knowledge of the geometry of the cavity is necessary. The cavity in our used map-section can be approximated by an ellipse with the projected distance 24.9 kpc from cluster center, projected semimajor axis with 20.5 kpc and semiminor axis with 12.4 kpc, as Wise et al. (2007) propose. Additionally the Hydra A north lobe is tilted by an angle θ towards the observer. Depending on θ the start of the Faraday active area in the model shifts. Fig. 4 shows that the sensitivity of our analysis starts at about 20 to 30 kpc from the cluster center depending on θ . θ is not well determined and ranges from about 30° (Taylor & Perley (1993), if cavity effect added) over 45° (Laing et al. 2008) to 60° (Wise et al. 2007).

3.3. Measuring the magnetic profile

The index α of the magnetic field can be retrieved from the data. In contrast to the power spectrum which is built dynamically by our algorithm, α has to be set up statically for every processing run. Maximizing the posterior with respect to α provides indications on most probable configurations. One drawback is that α also depends on the low-frequency cut-off k_{min} (position of the top of the first spectral bin) chosen; meaning a two dimensional problem needs to be optimized. The result we find is $\alpha = 1$ with $k_{min} = 0.42 \text{ kpc}^{-1}$. Since this result depends only on the large scales a rather low resolution study with 300 data points was sufficient and permitted a fast investigation of the 2-d parameter space. Sampling of k_{min} for three different projection angles θ can be found in Fig. 5. Cut-offs with $k < 0.42 \text{ kpc}^{-1}$ correspond to $\alpha > 1$ and vice versa. Smaller θ implies a smaller physical distance between the data points, which results in a small shift of k_{min} . However, it is negligible and inside the statistical variance of about 0.05 kpc^{-1} . Fig. 6 shows a consistency check by sampling α for the given $k_{min} = 0.42 \text{ kpc}^{-1}$. Altogether we deduce: $\alpha = 1 \pm 0.5$.

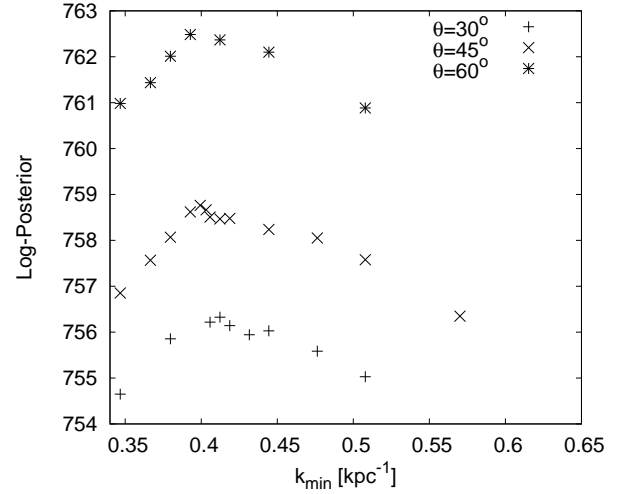


Fig. 5: Sampling of k_{min} for given $\alpha = 1$

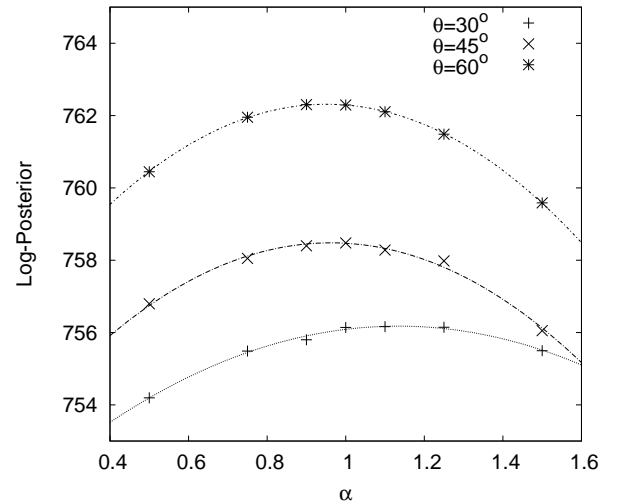


Fig. 6: Sampling of α for given $k_{min} = 0.42 \text{ kpc}^{-1}$

Surprisingly the maximum posterior is rising for rising θ with no apparent limit. We suppose that this has nothing to do with the probability of the physical model and therefore θ can not be restricted using the data of the Hydra A north lobe only. Indeed θ is a parameter, which only affects the integration bounds of Eq. 8, whereas the power spectrum, the magnetic scaling α and the cut-offs, affect the integrand.

3.4. Power spectrum and magnetic characteristics

The shape of the power spectrum depends on the spectral cut-offs k_{min} and k_{max} . We retrieved the most probable k_{min} to be 0.42 kpc^{-1} in Section 3.3. Obviously, the most probable configuration is a power law with no large scale turnover visible within the probed spatial scales as can be seen in Fig. 7. The decline for smaller k_{min} may be due to limited rotation measure map dimensions and the down-pull of thereby unconstrained amplitudes by Jeffrey's prior. A larger k_{min} will remove necessary degrees of freedom of the model at the large scales which forces to deposit additional power at the neighboring scale. The high-

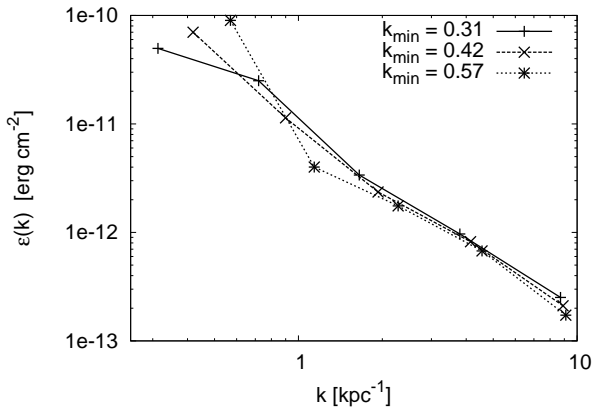


Fig. 7: Power spectrum with optimal, too small and too large cut-off k_{min}

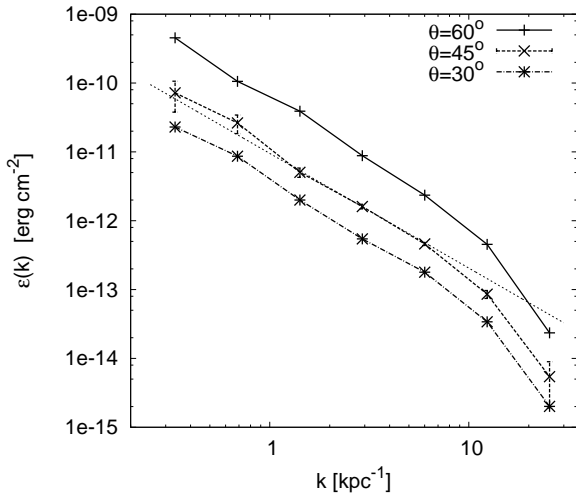


Fig. 8: Inferred power spectrum for three assumed projection angles and comparison with a Kolmogorov slope (dotted). Note that for $k > 10 \text{ kpc}^{-1}$ beam effects reduce the amount of power and should be responsible for the steepening.

frequency cut-off is limited by the resolution of the map and instrumental beam. A beam with spatial scales of 0.32 kpc gives $k_{min} = 10 \text{ kpc}^{-1}$. In the following, we increase the resolution by increasing the number of data points to 1000 and extend the spectrum to a maximal possible range. We do three processing runs with $\alpha = 1$ and three possible projection angles, see Fig. 8 and Table 1. To investigate the dependence of the results on α we do two more runs with $\alpha = 0.5$ and $\alpha = 1.5$, see Table 2. The given statistical uncertainties refer to static α and θ . Formulas for the calculation of the magnetic characteristics are described in Section B.

The power law ranges from scales of 0.3 kpc (beam FWHM) to about 8 kpc. The fall-off in power at small scales is due to instrumental beam effects. However, the larger scales are not greatly affected by the beam. To measure the spectral index we ignore the first spectral bin, which is possibly affected by map boundary limits as well as the last two beam affected bins. The dotted line in Fig. 8 represents a Kolmogorov slope of $\epsilon(k) \propto k^{-1.67}$ compared to the plot using $\theta = 45^\circ$. We get a perfect fit for the central part of the retrieved power spectrum, which

	B_o [μG]	B_{50} [μG]	λ_B [kpc]	spectral index
$\theta = 30^\circ$	21 ± 1	9.3	5.0 ± 1.0	1.70 ± 0.14
$\theta = 45^\circ$	36 ± 2	16	5.2 ± 1.1	1.73 ± 0.13
$\theta = 60^\circ$	85 ± 5	37	5.3 ± 1.2	1.85 ± 0.14

Table 1: Magnetic field characteristics for most probable $\alpha = 1$

	B_o [μG]	B_{50} [μG]	λ_B [kpc]	spectral index
$\alpha = 0.5^\circ$	18 ± 1	12	4.8 ± 1.1	1.56 ± 0.14
$\alpha = 1.5^\circ$	70 ± 4	21	5.5 ± 1.2	2.06 ± 0.14

Table 2: Magnetic field characteristics for $\theta = 45^\circ$ and maximal and minimal possible α

	α	B_o in μG	spectral index	large-scale turnover
Kuchar	1.0	36	1.73	no
Laing	0.25	19	0.8	no
Vogt	0.5	7.3	1.67	yes

Table 3: Recent results of Hydra A for $\theta = 45^\circ$

is also inside the larger statistical variance of the parts at smaller k . There is a noticeable dependence of the spectral index on α with minimal and maximal slopes of 1.5 and 2.1, which should be regarded as improbable worst cases. θ has a big impact on the resulting magnetic field strengths. Assuming a larger θ implies to a shorter interaction path with the magnetic field and therefore larger necessary magnetic field strengths. The derived B_o in the cluster center assumes that the magnetic profile given by Eq. 7 can be extrapolated with a constant α into the cluster center. However, the sensitivity starts at regions from about 30 kpc from cluster center, see Fig. 4 and a flattening of the magnetic profile at smaller radii is well possible. B_{50} gives the directly probed magnetic field strengths at 50 kpc distance.

The impact of the instrumental beam on the calculated magnetic field strength is low. A continuation of the power law to the small scales would give additional $0.2 \mu\text{G}$ at most.

4. Comparison with other methods

The magnetic power spectrum of Hydra A was previously measured by Vogt & Enßlin (2005) and by Laing et al. (2008). Both find significantly lower central magnetic field strengths than we do. This is due to a much flatter magnetic field profile inferred characterized by a smaller index α . Moreover Vogt & Enßlin (2005) found a bump, a cut-off at spatial scales of about 2 kpc and more, but the spectral index for small scales is still similar to our current results. However Laing finds a much flatter spectral index of about 0.8. Table 3 compares the results for a projection angle of $\theta = 45^\circ$.

To partly reconstruct the results of Vogt & Enßlin (2005), we apply the two simplifications in the calculation of the correlation matrix in Eq. 8, which they have used.

1. extending the second lower integration bound to $-\infty$
2. merging the two window functions f assuming the magnetic autocorrelation changes on much smaller scales than the window function

Then we compare the results to the Fourier method of Vogt, however extended with noise effects, cavity and a more advanced triangular parameterization of the power spectrum, see Fig. 9. We reconstruct the spectral bump found by Vogt & Enßlin (2005) and there is a perfect match between both methods. On the other

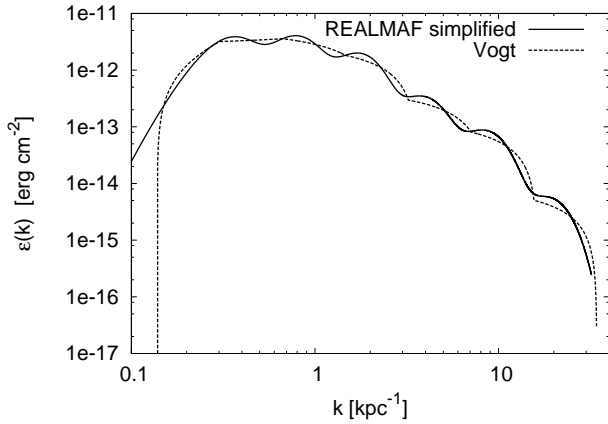


Fig. 9: Reconstructing of the results of the Fourier space method by Vogt & Enßlin (2005) by adding the removed simplifications for $\alpha = 0.5$ and $\theta = 45^\circ$. This plot illustrates the continuous result taking the model for the power spectrum into account.

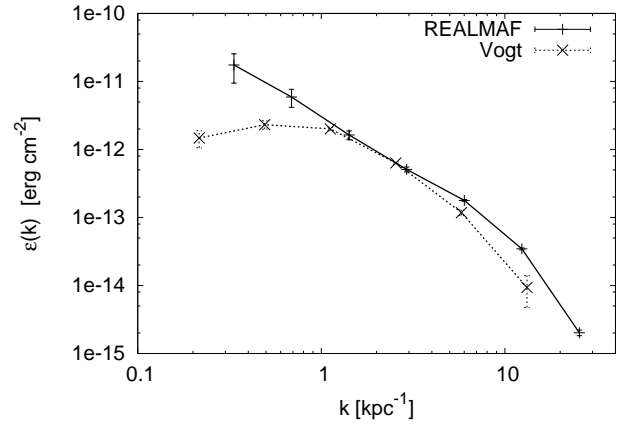


Fig. 10: Power spectrum with and without simplifications used in Vogt & Enßlin (2005) for $\alpha = 0.5$ and $\theta = 45^\circ$

hand Fig. 10 shows the difference to our method without these simplifications.

Consistent with Vogt the most likely α is shifted to much smaller values if one adopts these simplifications as can be seen in Fig.11. However instead of a falling plateau of the posterior between $\alpha = 0.1$ and $\alpha = 0.8$ and a cut-off for the unphysical range $\alpha < 0.1$ we find again a Gaussian distribution but with a maximum at 0.1. This very small α value indicates, that the bump found by Vogt & Enßlin (2005) may be explained by a power leak on large scales produced by an implicit increase of the large-scale contribution of the window function.

One of the major simplifications used by Laing et al. (2008) is a linear and position-independent relation between the RM power spectrum and the magnetic autocorrelation⁵, which is only valid for the case of a deep and statistical homogenous Faraday screen. Both assumptions are not very well met for the Hydra A cluster. If we simulate a constant electron density by setting $\alpha = -1$ and use symmetric integration bounds in Eq. 8 we get a spectral index of about 1.1. For $\alpha = 0.25$ we get a central magnetic field strength of $12.9 \mu G$, which is much closer to their results.

The remaining difference to the spectral index of 0.8 and field strength of $19 \mu G$ may be partly due to the beam correction applied by Laing et al. (2008), which lifts the high frequency part of the spectrum, which is possibly contaminated with noise residuals from the RM-map-making algorithms. An implementation of a beam correction as a convolution in real space is not feasible in REALMAF, because it would be computationally too expensive and an implementation in Fourier space is in general only possible with simplifying assumptions. However, the exact frequency dependent instrumental beam is unknown anyway, and we believe its effect can be neglected at scales larger than the beam length.

5. Conclusions

5.1. Summary

We developed a new method to retrieve magnetic power spectra from Faraday rotation maps implemented in the REALMAF

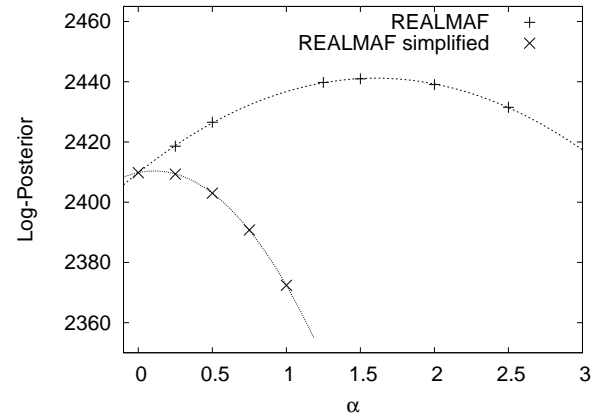


Fig. 11: Sampling of α with and without simplifications used in Vogt & Enßlin (2005) for $\theta = 45^\circ$ and $k_{min} = 0.3 \text{ kpc}^{-1}$

(REAL Magnetic Fields) code, where we modeled the magnetic autocorrelation function in real space.

Furthermore we introduced and verified a way to take the solenoidal character of the magnetic fields into account by using a simple full spherical model for the magnetic autocorrelation and multiplying with a proportionality factor. In contrast to the method by Vogt & Enßlin (2005) with a model in Fourier space, this permits to alleviate some previously required simplifications in the processing. However, we are able to reconstruct their results by synthetically adding these simplifications to our method.

Applied to the north lobe of the Hydra A galaxy cluster, we find a power law power spectrum in the spatial range of 0.3 kpc to 8 kpc, with no visible large-scale turnover within this range as reported by Vogt & Enßlin (2005). The magnetic density profile, which we modeled with an index α applied to the electron density profile, seems to follow the electron density profile with $\alpha = 1$. The statistical error of α of up to 0.5 is rather large and also influences the spectral index of the power law, which is then in the range of 1.5 to 2.1. The exact projection angle of the used radio lobe Hydra A north is not well restricted, but it only seriously affects the absolute value of the magnetic energy density in the cluster and not the spectral slope. Depending on the angle we get field strengths ranging from $20 \mu G$ up to $80 \mu G$ in the cluster center. However these are extrapolations, since the measurement is only sensitive at a distance of about 50 kpc from cluster center,

⁵ applied by Vogt & Enßlin (2003) as well

where we find fields between $10\mu G$ and $30\mu G$. The extrapolation of the model into the center may be questionable.

Theories describing the generation of magnetic fields by turbulence like Subramanian et al. (2006), Enßlin & Vogt (2006) and Schekochihin & Cowley (2006) forecast a large-scale turnover, which might be visible inside our spectral range. Compared to Vogt & Enßlin (2005) we found no large-scale turnover within the spectral range up to 8kpc. A turnover at larger scales is, however, not excluded by our analysis.

5.2. Outlook

The REALMAF code will permit to analyse the Faraday rotation data of further galaxy clusters. This will hopefully allow to study magnetic field spectra over a large range of spatial scales and in a variety of cluster environments. A usable map of Hydra A south would further increase the probed range at large scales and a map with a higher resolution would increase the range at small scales. We envisage a publication of the REALMAF code for general scientific usage. It might be possible to further improve the spectral parameterization, if one drops out the divergence relation in real space. Furthermore the divergence relation of a rescaled magnetic field might be expressed in a frequency dependent way to reflect the small deviations caused by the gradient of the rescale function.

Upcoming telescopes like EVLA, LOFAR, ASKAP and SKA will certainly provide the necessary high fidelity Faraday rotation data of many more galaxy clusters for further studies with REALMAF. This may help to figure out the origin of cluster magnetic fields and the role they play in the metabolism of the intra-cluster medium.

Acknowledgements. Special thanks to Corina Vogt, who made her code used in Vogt & Enßlin (2005) available for insight. Thanks to Daria Guidetti and Robert Laing for discussions.

Appendix A: Model functions

Here we describe the construction of our spectral model functions. We start with an ansatz for $M_L(r)$ for the case $\nabla \cdot \tilde{B} = 0$ and use a Gaussian multiplied with a cosine. The corresponding $M_N(r)$ is obtained by Equation 13. Thus we adopt:

$$\begin{aligned} M_L^{(i)}(r) &= \frac{1}{\sqrt{2\pi}} b_i^3 \exp\left[-\frac{1}{2} \frac{r^2}{a_i^2}\right] \cos[b_i r], \text{ and} \\ M_N^{(i)}(r) &= \frac{b_i^3}{2a_i^2 \sqrt{2\pi}} \exp\left[-\frac{r^2}{2a_i^2}\right] \left[(2a_i^2 - r^2) \cos[b_i r] \right. \\ &\quad \left. + a_i^2 b_i r \sin[b_i r] \right]. \end{aligned} \quad (\text{A.1})$$

These functions are Fourier transformed analytically using:

$$M(k) = 4\pi \int_0^\infty r^2 M(r) \frac{\sin[kr]}{kr} dr,$$

see Enßlin & Vogt (2003). We bind the free parameter a_i as

$$a_i = \frac{3}{4} b_i,$$

because in this case $\omega^{(i)}(k) = 2M_N^{(i)}(k) + M_L^{(i)}(k)$ is fully positive and concentrated around a maximum at $k = 3b_i$. This allows us to put the power spectrum together by relatively well separated and located frequency bands, as Fig. A.2 illustrates. Fig. A.1 shows the model functions in position space. Especially $M_N(r)$

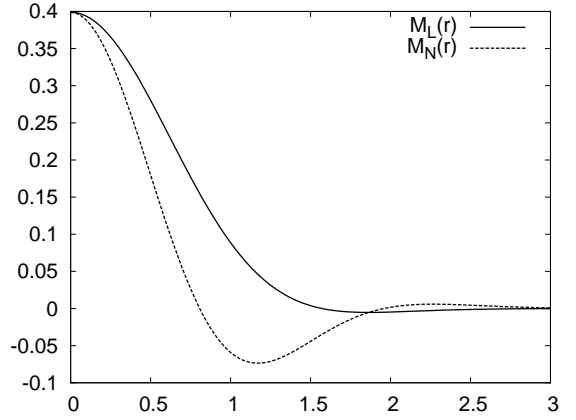


Fig. A.1: model functions $M_N^{(i)}(r)$ and $M_L^{(i)}(r)$ with $a_i = \frac{3}{4}$ and $b_i = 1$

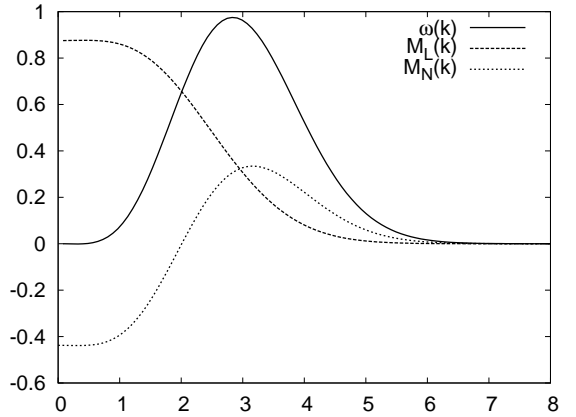


Fig. A.2: Model functions $M_N^{(i)}(k)$, $M_L^{(i)}(k)$ and $\omega^{(i)}(k)$ in Fourier space with $a_i = \frac{3}{4}$ and $b_i = 1$

has a strong negative part, due to the fact that any closed field line has to come somewhere back through the plane perpendicular to it.

If we assume full isotropy, $M_{zz}(r)$ gets spherically symmetric. In this case a suitable model function can be obtained by Eq. A.1:

$$M_{zz}^{(i)}(r) = \frac{1}{3} \omega^{(i)}(r) = \frac{1}{3} (M_L^{(i)}(r) + 2M_N^{(i)}(r)) \quad (\text{A.2})$$

This implicitly assumes $M_N(r) = M_L(r)$. Thus we get

a) using $\nabla \cdot \tilde{B} = 0$
in position space:

$$\begin{aligned} M_L^{(i)}(r) &= \frac{b_i^3}{\sqrt{2\pi}} \exp\left[-\frac{8}{9} b_i^2 r^2\right] \cos[b_i r] \\ M_N^{(i)}(r) &= \frac{b_i^3}{18 \sqrt{2\pi}} \exp\left[-\frac{8}{9} b_i^2 r^2\right] \left[(2(9 - 8b_i^2 r^2) \cos[b_i r] \right. \\ &\quad \left. - 9b_i r \sin[b_i r] \right) \end{aligned} \quad (\text{A.3})$$

in Fourier space:

$$\begin{aligned}
M_L^{(i)}(k) &= \frac{27}{64}\pi \left(\frac{k-b_i}{k} \exp\left[-\frac{9(b_i-k)^2}{32b_i^2}\right] \right. \\
&\quad \left. + \frac{k+b_i}{k} \exp\left[-\frac{9(b_i+k)^2}{32b_i^2}\right] \right) \\
M_N^{(i)}(k) &= \frac{27}{128}\pi \left(\left(\frac{9(b_i-k)^2}{16b_i^2} - 1 \right) \exp\left[-\frac{9(b_i-k)^2}{32b_i^2}\right] \right. \\
&\quad \left. + \left(\frac{9(b_i+k)^2}{16b_i^2} - 1 \right) \exp\left[-\frac{9(b_i+k)^2}{32b_i^2}\right] \right)
\end{aligned} \tag{A.4}$$

and

b) using full isotropy
in position space:

$$\begin{aligned}
M_{zz}^{(i)}(r) &= \frac{b_i^3}{27\sqrt{2\pi}} \exp\left[-\frac{8}{9}b_i^2r^2\right] \\
&\quad \cdot \left((27 - 16b_i^2r^2) \cos[b_i r] - 9b_i r \sin[b_i r] \right)
\end{aligned} \tag{A.5}$$

in Fourier space:

$$\begin{aligned}
M_{zz}^{(i)}(k) &= \frac{27}{1024b_i^2k} \pi \exp\left[-\frac{9(b_i+k)^2}{32b_i^2}\right] \\
&\quad \left(16b_i^3 + 9b_i^2k + 18b_i k^2 + 9k^2 + 9k^3 \right) \\
&\quad + \exp\left[\frac{9k}{8b_i}\right] \left(-16b_i^3 + 9b_i^2k - 18b_i k^2 + 9k^3 \right).
\end{aligned} \tag{A.6}$$

Appendix B: Calculation of magnetic field characteristics

Here we provide the used formula for the magnetic field characteristics.

a) Magnetic field strength

The magnetic energy density can be calculated by integrating over the power spectrum or analogously taking the autocorrelation function in real space at the origin $\omega(0)$. The magnetic field strength in the center of the cluster, where $f = 1$ and therefore $\tilde{B} = B$, is then:

$$B = \sqrt{\omega(0)} \tag{B.1}$$

b) Magnetic autocorrelation length

$$\lambda_B = \frac{\int_{-\infty}^{\infty} dr \omega(r)}{\omega(0)} \tag{B.2}$$

c) 1-dimensional power spectrum

Transformation from the 3-dimensional power spectrum $\omega(k)$ to the one-dimensional $\epsilon(k)$ is done using (Enßlin & Vogt 2003)

$$\epsilon(k) = \frac{k^2 \omega(k)}{2(2\pi)^3} \tag{B.3}$$

d) Spectral index using a Bayesian approach

The spectral index can be calculated from the slope of the power spectrum in logarithmic scale. The fitting formula is:

$$\epsilon(k) = \epsilon_o \left(\frac{k}{k_o} \right)^{-r} = qk^{-r}$$

The variance from the above power law is then defined as:

$$\delta s = s_i - qk_i^{-r}$$

The allowed statistical deviations of s are imprinted in a covariance matrix $D_{ij} = \langle \delta s_i \delta s_j \rangle$, which is automatically obtained from the inverse of the Hessian matrix calculated with the maximum a posteriori approach as described in Section 2.2. The probabilities of the spectral amplitudes s of the power spectrum can be approximated as a Gaussian, where we can neglect the normalization factor, because it is independent on q and r :

$$P(\delta s|q, r) \propto e^{-\frac{1}{2}\delta s^T D_{ij}^{-1} \delta s}$$

Only a part of the power spectrum is used to fit the power law. D_{ij} is then the projection (cut) of the full inverse Hessian matrix \tilde{D}_{ij} obtained from Eq. 6.:

$$D_{ij} = \langle \delta s_i \delta s_j \rangle = \psi^T \tilde{D}_{ij} \psi,$$

with the projection operator $\psi = \{0, \dots, 1, \dots, 1, \dots, 0\}$ selecting the used spectral bins for the fit. Using the Bayesian theorem from Eq. 3:

$$P(q, r|\delta s) \propto P(\delta s|q, r),$$

where we already applied a uniform prior distribution $P(r, q) = \text{const}$. $P(q, r|\delta s)$ has to be maximized to get the desired slope r within a maximum a posteriori approach. To find the optimum numerically the gradients and the 2x2 Hessian matrix are necessary:

$$\frac{\partial \ln P}{\partial r} = -q \ln[k_i] k_i^{-r} D_{ij}^{-1} (s_j - qk_j^{-r})$$

$$\frac{\partial \ln P}{\partial q} = k_i^{-r} H_{ij}^{-1} (s_j - qk_j^{-r})$$

$$\frac{\partial^2 \ln P}{\partial q^2} = -k_i^{-r} D_{ij}^{-1} k_j^{-r}$$

$$\begin{aligned} \frac{\partial^2 \ln P}{\partial r^2} &= q(q \ln[k_i] k_i^{-r} D_{ij}^{-1} \ln[k_j] k_j^{-r} \\ &\quad - (\ln[k_i])^2 k_i^{-r} D_{ij}^{-1} (s_j - qk_j^{-r})) \end{aligned}$$

$$\frac{\partial^2 \ln P}{\partial q \partial r} = 2q \ln[k_i] k_i^{-r} D_{ij}^{-1} k_j^{-r} - \ln[k_i] k_i^{-r} D_{ij}^{-1} s_j$$

An expression for the second unknown q can be found analytically. If the initial value of r is given, then the corresponding initial value q can be calculated easily. This is necessary because the first guess must be close to the maximum to get convergence.

$$q = \frac{k_i^{-r} D_{ij}^{-1} s_j}{k_i^{-r} D_{ij}^{-1} k_j^{-r}}$$

References

- Battaglia, N., Frommer, C., Sievers, J. L., Bond, J. R., & Enßlin, T. A. 2009, MNRAS, 393, 1073
Boehringer, H., Voges, W., Fabian, A. C., Edge, A. C., & Neumann, D. M. 1993, MNRAS, 264, L25
Carilli, C. L. & Taylor, G. B. 2002, ARA&A, 40, 319
Cho, J. & Ryu, D. 2009, ApJ, 705, L90
Clarke, T. E., Kronberg, P. P., & Böhringer, H. 2001, ApJ, 547, L111
David, L. P., Nulsen, P. E. J., McNamara, B. R., et al. 2001, ApJ, 557, 546
de Vaucouleurs, G., de Vaucouleurs, A., Corwin, Jr., H. G., et al. 1991, Third Reference Catalogue of Bright Galaxies

- Dennison, B. 1979, *AJ*, 84, 725
- Dolag, K., Bartelmann, M., & Lesch, H. 2002, *A&A*, 387, 383
- Dolag, K., Schindler, S., Govoni, F., & Feretti, L. 2001, *A&A*, 378, 777
- Dolag, K., Vogt, C., & Enßlin, T. A. 2005, *MNRAS*, 358, 726
- Dreher, J. W., Carilli, C. L., & Perley, R. A. 1987, *ApJ*, 316, 611
- Eilek, J. A. & Owen, F. N. 2002, *ApJ*, 567, 202
- Enßlin, T. A. 1999, in *Diffuse Thermal and Relativistic Plasma in Galaxy Clusters*, ed. H. Boehringer, L. Feretti, & P. Schuecker, 275
- Enßlin, T. A. & Vogt, C. 2003, *A&A*, 401, 835
- Enßlin, T. A. & Vogt, C. 2006, *A&A*, 453, 447
- Enßlin, T. A., Vogt, C., Clarke, T. E., & Taylor, G. B. 2003, *ApJ*, 597, 870
- Fabian, A. C., Sanders, J. S., Ettori, S., et al. 2000, *MNRAS*, 318, L65
- Feain, I. J., Ekers, R. D., Murphy, T., et al. 2009, *ApJ*, 707, 114
- Feretti, L., Dallacasa, D., Giovannini, G., & Tagliani, A. 1995, *A&A*, 302, 680
- Feretti, L., Dallacasa, D., Govoni, F., et al. 1999a, *A&A*, 344, 472
- Feretti, L., Perley, R., Giovannini, G., & Andernach, H. 1999b, *A&A*, 341, 29
- Ge, J. & Owen, F. N. 1994, *AJ*, 108, 1523
- Goldshmidt, O. & Rephaeli, Y. 1993, *ApJ*, 411, 518
- Govoni, F., Murgia, M., Feretti, L., et al. 2006, *A&A*, 460, 425
- Guidetti, D., Murgia, M., Govoni, F., et al. 2008, *A&A*, 483, 699
- Hennessy, G. S., Owen, F. N., & Eilek, J. A. 1989, *ApJ*, 347, 144
- Johnson, R. A., Leahy, J. P., & Garrington, S. T. 1995, *MNRAS*, 273, 877
- Johnston-Hollitt, M., Hollitt, C. P., & Ekers, R. D. 2004, in *The Magnetized Interstellar Medium*, ed. B. Uyaniker, W. Reich, & R. Wielebinski, 13–18
- Kim, K., Kronberg, P. P., & Tribble, P. C. 1991, *ApJ*, 379, 80
- Laing, R. A. 1988, *Nature*, 331, 149
- Laing, R. A., Bridle, A. H., Parma, P., & Murgia, M. 2008, *MNRAS*, 391, 521
- Laing, R. A., Canvin, J. R., Cotton, W. D., & Bridle, A. H. 2006, *MNRAS*, 368, 48
- Lawler, J. M. & Dennison, B. 1982, *ApJ*, 252, 81
- McNamara, B. R., Wise, M., Nulsen, P. E. J., et al. 2000, *ApJ*, 534, L135
- Mohr, J. J., Mathiesen, B., & Evrard, A. E. 1999, *ApJ*, 517, 627
- Murgia, M., Govoni, F., Feretti, L., et al. 2004, *A&A*, 424, 429
- Schekochihin, A. A. & Cowley, S. C. 2006, *Physics of Plasmas*, 13, 056501
- Subramanian, K. 1999, *Physical Review Letters*, 83, 2957
- Subramanian, K., Shukurov, A., & Haugen, N. E. L. 2006, *MNRAS*, 366, 1437
- Taylor, G. B., Fabian, A. C., & Allen, S. W. 2002, *MNRAS*, 334, 769
- Taylor, G. B., Fabian, A. C., Gentile, G., et al. 2007, *MNRAS*, 382, 67
- Taylor, G. B., Govoni, F., Allen, S. W., & Fabian, A. C. 2001, *MNRAS*, 326, 2
- Taylor, G. B. & Perley, R. A. 1993, *ApJ*, 416, 554
- Taylor, G. B., Perley, R. A., Inoue, M., et al. 1990, *ApJ*, 360, 41
- Vogt, C., Dolag, K., & Enßlin, T. A. 2005, *MNRAS*, 358, 732
- Vogt, C. & Enßlin, T. A. 2003, *A&A*, 412, 373
- Vogt, C. & Enßlin, T. A. 2005, *A&A*, 434, 67
- Wise, M. W., McNamara, B. R., Nulsen, P. E. J., Houck, J. C., & David, L. P. 2007, *ApJ*, 659, 1153
- Xu, Y., Kronberg, P. P., Habib, S., & Dufton, Q. W. 2006, *ApJ*, 637, 19